

<https://helda.helsinki.fi>

---

## Promoting Cardiac Repair through Simple Engineering of Nanoparticles with Exclusive Targeting Capability toward Myocardial Reperfusion Injury by Thermal Resistant Microfluidic Platform

Liu, Zehua

2022-09

---

Liu , Z , Lian , W , Long , Q , Cheng , R , Torrieri , G , Zhang , B , Koivuniemi , A , Mahmoudzadeh , M , Bunker , A , Gao , H , He , H , Chen , Y , Hirvonen , J , Zhou , R , Zhao , Q , Ye , X , Deng , X & Santos , H A 2022 , ' Promoting Cardiac Repair through Simple Engineering of Nanoparticles with Exclusive Targeting Capability toward Myocardial Reperfusion Injury by Thermal Resistant Microfluidic Platform ' , *Advanced Functional Materials* , vol. 32 , no. 36 , 2204666 . <https://doi.org/10.1002/adfm.202204666>

---

<http://hdl.handle.net/10138/351014>

<https://doi.org/10.1002/adfm.202204666>

---

cc\_by

publishedVersion

---

*Downloaded from Helda, University of Helsinki institutional repository.*

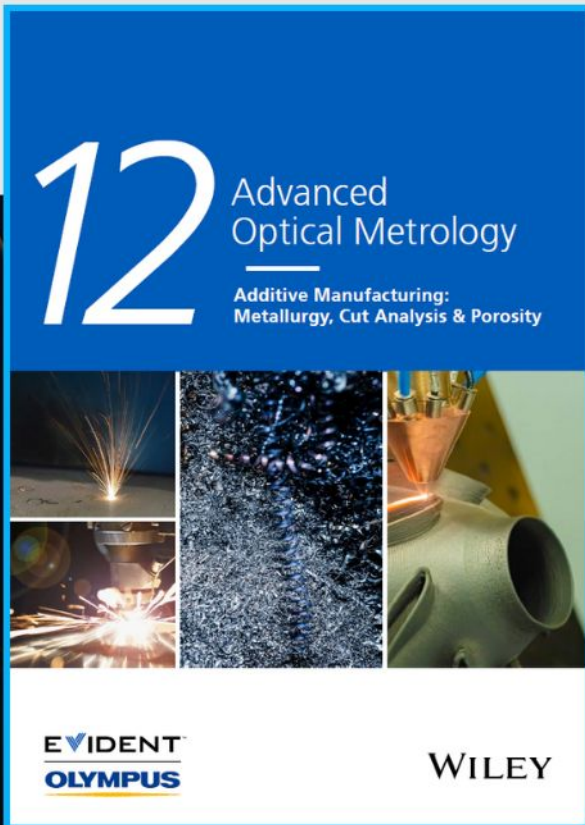
*This is an electronic reprint of the original article.*

*This reprint may differ from the original in pagination and typographic detail.*

*Please cite the original version.*



# Additive Manufacturing: Metallurgy, Cut Analysis & Porosity



The latest eBook from  
**Advanced Optical Metrology.**  
Download for free.

In industry, sector after sector is moving away from conventional production methods to additive manufacturing, a technology that has been recommended for substantial research investment.

Download the latest eBook to read about the applications, trends, opportunities, and challenges around this process, and how it has been adapted to different industrial sectors.

**EVIDENT™**  
**OLYMPUS**

**WILEY**

# Promoting Cardiac Repair through Simple Engineering of Nanoparticles with Exclusive Targeting Capability toward Myocardial Reperfusion Injury by Thermal Resistant Microfluidic Platform


Zehua Liu, Wenhua Lian, Qiang Long, Ruoyu Cheng, Giulia Torrieri, Baoding Zhang, Artturi Koivuniemi, Mohammad Mahmoudzadeh, Alex Bunker, Han Gao, Hongbin He, Yun Chen, Jouni Hirvonen, Rongbin Zhou, Qiang Zhao,\* Xiaofeng Ye,\* Xianming Deng,\* and Hélder A. Santos\*

Nanoparticle (NP)-based intravenous administration represents the most convenient cardiac targeting delivery routine, yet, there are still therapeutic issues due to the lack of targeting efficiency and specificity. Active targeting methods using functionalization of ligands onto the NPs' surface may be limited by trivial modification procedures and reduced targeting yield *in vivo*. Here, a microfluidics assisted single step, green synthesis method is introduced for producing targeting ligands free heart homing NPs in a tailored manner. The generated  $\beta$ -glucan-based NPs exhibit precise and efficient targeting capability toward Dectin-1<sup>+</sup> monocytes/macrophages, which are confirmed as main pathogenesis mediators for cardiac ischemic/reperfusion (I/R) injury, with a sequentially enhanced cardiac NP accumulation, and this targeting strategy is exclusively suitable for cardiac I/R but not for other cardiovascular diseases, as confirmed both in murine and human model. Comparing to FDA-approved nano-micelles formulation,  $\beta$ -glucan NPs loaded with NACHT, LRR, and PYD domains-containing protein 3 (NLRP3) inflammasome inhibitor (CY-09) exhibit better efficiency in ameliorating myocardial injury and heart failure induced by surgically induced I/R. These findings indicate a simple production of targeting-ligand free NPs, and demonstrate their potential therapeutic applications for preclinical I/R-induced cardiac injury amelioration.

## 1. Introduction

Cardiovascular diseases were, and still will be the leading cause of death globally.<sup>[1]</sup> Adopting heart targeting nanoparticles (NPs) for cardiac diseases has several unique advantages. Foremost, it is totally non-invasive and is so far the most convenient method for targeted delivery to heart, especially to specific immune cells subsets, such as monocytes and macrophages.<sup>[2]</sup> This flexibility further confers a feasible control over the dosing regimen in regarding to administration time and course of treatment, making it suitable for therapeutic modalities that have narrow or particular therapeutic window.<sup>[2b,c]</sup> However, to target specific cell-subsets, extra functionalization of the NPs by targeting moieties are usually needed.<sup>[3]</sup> In addition to the potentially reduced targeting yield *in vivo*,<sup>[4]</sup> the trivial modification process of the NPs and the issue in batch-to-batch variation may hinder the clinical translation of such strategy to some extent.<sup>[5]</sup> Therefore, synthesizing

Z. Liu, W. Lian, B. Zhang, Y. Chen, X. Deng  
State Key Laboratory of Cellular Stress Biology  
Innovation Center for Cell Biology  
School of Life Sciences  
Xiamen University  
Xiamen 361102, China  
E-mail: xmdeng@xmu.edu.cn

 The ORCID identification number(s) for the author(s) of this article can be found under <https://doi.org/10.1002/adfm.202204666>.

© 2022 The Authors. Advanced Functional Materials published by Wiley-VCH GmbH. This is an open access article under the terms of the Creative Commons Attribution-NonCommercial License, which permits use, distribution and reproduction in any medium, provided the original work is properly cited and is not used for commercial purposes.

DOI: 10.1002/adfm.202204666

Z. Liu, R. Cheng, H. Gao, H. A. Santos  
Department of Biomedical Engineering  
University Medical Center Groningen/University of Groningen  
A. Deusinglaan 1, 9713 AV Groningen, Netherlands  
E-mail: h.a.santos@umcg.nl

Z. Liu, R. Cheng, H. Gao, H. A. Santos  
W.J. Kolff Institute for Biomedical Engineering and Materials Science  
University Medical Center Groningen

Ant. Deusinglaan 1, 9713 AV Groningen, The Netherlands

Z. Liu, G. Torrieri, H. Gao, J. Hirvonen, H. A. Santos  
Drug Research Program  
Division of Pharmaceutical Chemistry and Technology  
Faculty of Pharmacy  
University of Helsinki  
FI-00014 Helsinki, Finland

targeting ligands free NPs with inherent heart homing capability in a simple, convenient, and robust manner is preferred.

Recent insights into cardiovascular immunopathology have shifted therapeutic focus to manipulating the maladaptive innate immune responses.<sup>[6]</sup> In a recent clinical study, Dectin-1<sup>+</sup> monocytes/macrophages were shown as the major and particular pathogenesis mediators for myocardial ischemic/reperfusion (I/R) injury.<sup>[7]</sup> However, simply abolishing Dectin-1 expression will induce severe side effects,<sup>[8]</sup> therefore strategies to effectively and specifically sequester detrimental functions of Dectin-1<sup>+</sup> monocytes/macrophages are speculated to be the orientation for further studies.  $\beta$ -glucans are inherent Dectin-1 ligands with high affinity and specificity,<sup>[9]</sup> and have also been widely applied as drug delivery vehicles or immune adjuvants,<sup>[10]</sup> but their applications for I/R-induced myocardial injury are less investigated. Thus, we hypothesize that  $\beta$ -glucan based NPs can effectively load therapeutic cargos for specifically sequestering detrimental functions of Dectin-1<sup>+</sup> monocytes/macrophages (Figure 1a,b). However, the conventional  $\beta$ -glucan NPs fabrication methods, such as metal immobilization or thermal denaturation,<sup>[11]</sup> usually involve with complex scheme, harsh condition, and organic solvent. Thus, new strategy for green synthesizing  $\beta$ -glucan NPs in a simple, robust, and economically feasible manner should be proposed to fulfill the potential pharmaceutical formulation requirements.

Herein, we established a green synthesis routine for producing heart targeting NPs from phosphorylated barley  $\beta$ -1,3-1,4 glucan (PG, Figure S1, Supporting Information). A modified glass-capillary microfluidic platform (overall cost less than one U.S. dollar per chip) is introduced to tailor the physiochemical characters of the produced NPs. Comparing to conventional bulk method, the currently purposed NPs production method is in a continuous manner, with significantly reduced size and batch-to-batch variation, which are critical factors for potential clinical translation.<sup>[12]</sup> Critical physiochemical factors governing the NPs formation and properties were investigated and confirmed in silico. An novel kinase inhibitor (CY-09) was screened and sequentially encapsulated in the NPs (termed as CY-09@CG)

with high loading capacity to interrupt NACHT, LRR, and PYD domains-containing protein 3 (NLRP3) inflammasome activation,<sup>[13]</sup> as previous studies suggested Dectin-1-mediated immunoactivation is linked to the proteolytic functions of NLRP3 inflammasome to maximize the bioactive of IL-1 $\beta$ .<sup>[14]</sup> We confirmed biocompatibility of the current NPs for cardiac diseases, and enhanced cardiac NPs accumulation post myocardial I/R. We sequentially suggested this targeting strategy might be exclusively suitable for cardiac I/R but not for other cardiovascular diseases, which was confirmed both in murine and human model. Last, we confirmed that the drug loaded NPs outperformed the conventional nano-micelles formulation in regarding to subsiding reperfusion injury and preserving cardiac function in long term. Our study highlights an easy, economical feasible and simple yet robust synthesis procedure of  $\beta$ -glucan based NPs for I/R-induced cardiac injury, which showed great clinical translational potential as an alternative post-conditioning routine after the revascularization surgery.

## 2. Results and Discussion

### 2.1. Fabrication of $\beta$ -Glucan Nanoparticles via Microfluidics

Considering the potential application in I/R injury treatment, we hypothesized the developed  $\beta$ -glucan NPs would provide the following features: 1) Simple and robust production method for achieving low batch-to-batch variations; 2)  $\approx$ 100 nm size with good stability for enhancing macrophages phagocytosis and leaky endothelium permeation;<sup>[15]</sup> and 3) inherent yet specific targeting capability of the starting materials for avoiding extra targeting modifications on the surface of the NPs. Herein, barley  $\beta$ -1,3-1,4 glucan ( $M_w = 179\ 000\ \text{g mol}^{-1}$ ) was first modified into PG (Figure S1a, Supporting Information),<sup>[16]</sup> and the phosphorylation efficiency was calculated to be 28.7% based on the phosphate-nuclear magnetic resonance (P-NMR) results (Figure S1b, Supporting Information). PG spontaneously formed into NPs with chitosan (CS) in aqueous condition without participation of organic solvent. To optimize the formulation design, we constructed a series of CS/PG (CG) NPs with different CS-to-PG ratio (wt/wt), and measured their corresponding surface zeta ( $\zeta$ )-potential (Figure S2a, Supporting Information). We observed that CG NPs with positive surface charges were not colloidal-stable under neutral-alkaline solutions (data not shown), therefore we chose an initial set of  $0.4\ \text{mg mL}^{-1}$  of CS and  $0.8\ \text{mg mL}^{-1}$  of PG for further CG NPs synthesized ( $\zeta$ -potential =  $-21\ \text{mV}$ ). However, as a result of the high molecular weight and viscosity (11 cSt) of barley  $\beta$ -glucan,<sup>[17]</sup> the size and polydispersity index (PDI) of the produced NPs via a bulk method were high ( $257 \pm 34\ \text{nm}$ ,  $0.29 \pm 0.01$ , Figure 1c), as measured by dynamic light scattering (DLS). Despite by increasing the synthesis temperature to  $65\ ^\circ\text{C}$ , the size of the CG NPs was reduced to  $212 \pm 25\ \text{nm}$  (PDI =  $0.38 \pm 0.07$ , Figure 1c), this size is still relative large and may impede macrophage uptake efficiency.<sup>[15]</sup> Thus, we employed a microfluidic technique, known to have the capability to reduce the size and PDI of the produced NPs.<sup>[17,18]</sup> However, using a conventional co-flow flow-focusing glass capillary microfluidic chip (Figure 1d), the size and PDI of the CG NPs was not significantly altered ( $228 \pm 49\ \text{nm}$ ,  $0.30 \pm 0.06$ ,

Z. Liu, W. Lian, B. Zhang, Y. Chen, X. Deng  
State-Province Joint Engineering Laboratory of Targeted Drugs from  
Natural Products

School of Life Sciences  
Xiamen University  
Xiamen 361102, China

Q. Long, Q. Zhao, X. Ye  
Department of Cardiovascular Surgery  
Ruijin Hospital

Shanghai Jiaotong University School of Medicine  
Shanghai 200000, China  
E-mail: zq11607@rjh.com.cn; yxf11612@rjh.com.cn

A. Koivuniemi, M. Mahmoudzadeh, A. Bunker  
Division of Pharmaceutical Biosciences  
Faculty of Pharmacy  
University of Helsinki  
FI-00014 Helsinki, Finland

H. He, R. Zhou  
Institute of Immunology and the CAS Key Laboratory of Innate Immunity  
and Chronic Disease  
CAS Center for Excellence in Molecular Cell Sciences  
School of Life Sciences and Medical Center  
University of Science and Technology of China  
Hefei 230000, China

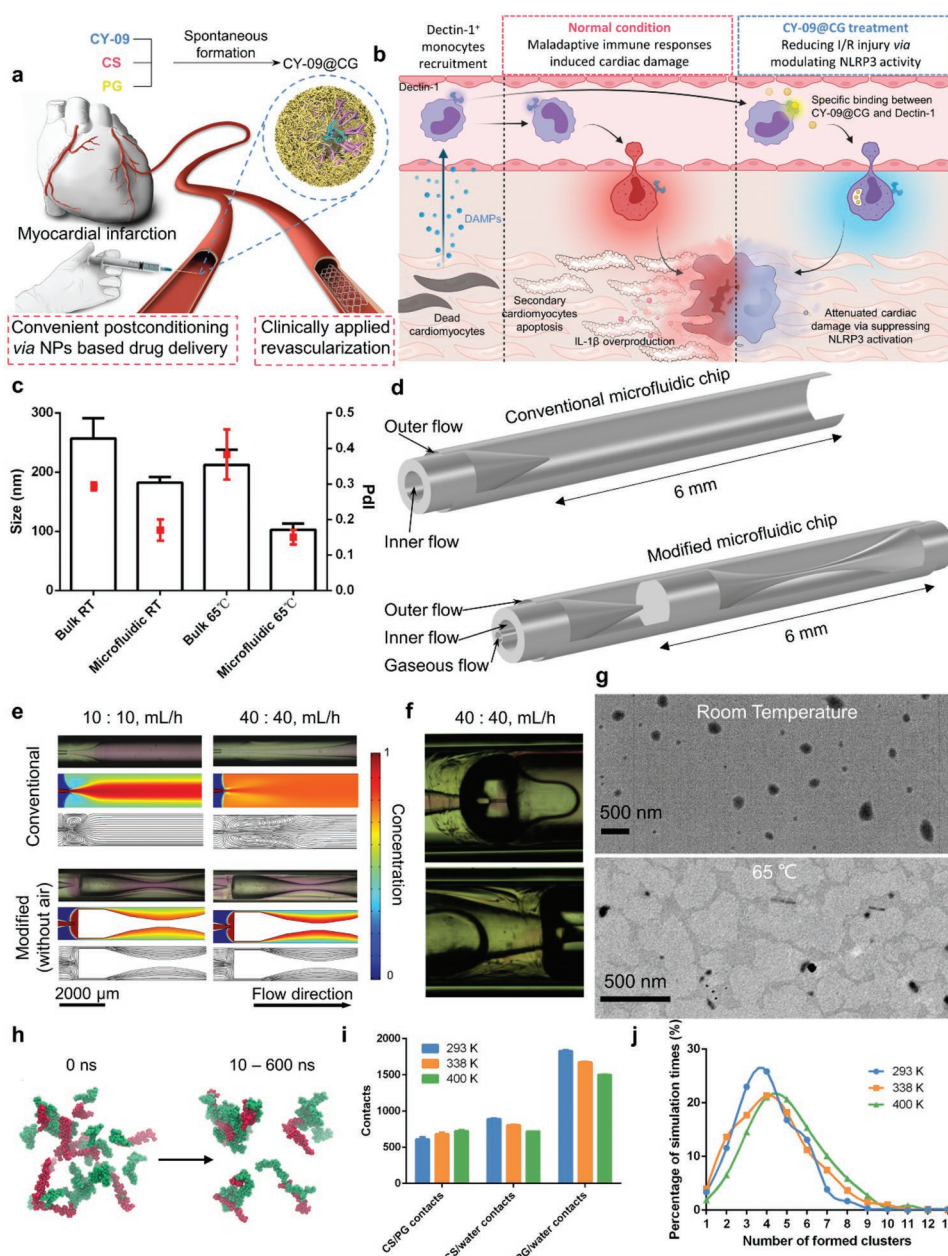


**Figure 1.** Schematic illustration of the concept of the current study, and the corresponding fabrication/characterization of CG NPs produced via microfluidics. a) Clinical application scenario of NP-based drug delivery for I/R-induced cardiac damage. b) Schematic showing the principle of design of the current system. Dectin-1 targeting NPs will sequentially modulate the maladaptive immune responses from macrophages for inhibiting the secondary myocardial injury. c) Size and PDI of the CG NPs produced by different methods and at different temperatures. Black histogram indicates the size data, while the red dots indicate the corresponding PDI. All data in the graphs are shown as mean  $\pm$  SD from three independent replicates. d) 3D model for the conventional and modified microfluidic chips tested. The distance between the inner orifice and the mixing compartment in the modified microfluidic chip was set as 200  $\mu\text{m}$ . The diameter of outer fluidic channel, inner fluidic channel, gaseous channel and orifice was 1000, 580, 100, and 80  $\mu\text{m}$ , respectively. e) Fluidic mixing and corresponding computational fluid dynamic simulations. Distribution of the normalized solvent concentration at a flow rate (FR) of 10:10, and 40:40 ( $\text{mL h}^{-1}$ ) for the conventional microfluidic chip and the modified microfluidic chip without gas phase. Phenol red is used as the mixing indicator for real-time optical imaging (up). The color bar represents the normalized concentration magnitude within the computational domain (middle), and the contour represents the fluid velocity magnitude (down). f) Microscopic view of a transparent microchannel, showing the vortices in the segmented gas-liquid flow at the FR of 40:40. The wall friction in the channel causes a relative backflow of the liquid so that it circulates symmetrically around the central axes of the channel in the form of vortices. g) Representative TEM images of CG NPs synthesized at room temperature (up) and 65  $^{\circ}\text{C}$  (down). h) Snapshots from the top-clusters acquired from all-atom molecular dynamics simulations of CG NP formation process. The polymer chain composed by green beads represents chitosan (CS); polymer chain composed by red beads represents phosphorylated  $\beta$ -glucan (PG). i, j) Molecular dynamics simulation results demonstrated the higher temperature led to increased CS/PG contacts (i) and the higher number of cluster formation (j), which achieved an overall smaller size of produced NPs. Values are expressed as the mean  $\pm$  SD of three independent calculations. NPs, nanoparticles; CS, chitosan; PG, phosphorylated barley  $\beta$ -1,3-1,4 glucan; DAMPs, damage associated molecular patterns; NLRP3, NACHT, LRR, and PYD domains-containing protein 3.

Figure S2b, Supporting Information). This is mainly due to the restrained mixing efficiency under relatively low flow rate (FR, Figure 1e and Figure S2c, Supporting Information).<sup>[12,17]</sup> Therefore, we further designed a thermal-resistant glass-capillary microfluidic chip (Figure 1d) to solve the problem, using a two-step modification approach. The first-step consists in the insertion of an hourglass-shaped glass compartment in the mixing channel, which only sparingly improved the mixing efficiency under different FR ratio (Figure 1e and Figure S2c, Supporting Information). Sequentially, a chaotic advection was achieved by creating a periodic two-phase flow via segmenting the continuous flow with the immiscible medium (air).<sup>[19]</sup> This simple and cost-effective chip generated a gaseous slugs to create an unsteady flow condition as reflected by the streamlines of the continuous fluid, yielding a fast homogenous mixing (<40 ms) at low FR (inner FR/outer FR = 40/40, mL h<sup>-1</sup>, Figure 1f). As a result, CG NPs with the size of 182 ± 9 nm were fabricated with the modified microfluidic chip at room temperature. Due to the thermal-resistant behavior of this microchip, we could synthesize the NP at the temperature of 65 °C, and the size of the CG NPs was reduced to 102 ± 10 nm (Figure 1c). In concordance with the hydrodynamic diameter obtained from the DLS results, transmission electron microscopy (TEM) images also showed sub-100 nm size of the produced NPs, which indicate a distinct difference comparing to the CG NPs synthesized under room temperature (Figure 1g). Colloidal stability is crucial for potential therapeutic applications, and the produced CG NPs showed a satisfied colloidal stability in terms of sizes and PDI after 1 month storage in saline solution (pH = 7.4) at 37 °C (Figure S2d,e, Supporting Information).

We next carried out molecular dynamics simulations to gain insights on the mechanism of the high temperature effect on the synthesis of the CG NPs (Figure S3a,b, Supporting Information). CG NPs were spontaneously formed through ionic gelation (Figure 1h). While the radius of gyration (indicator for specific molecule volume, Figure S3c, Supporting Information) of both CS and PG chain was kept constant under all temperatures, the temperature increase positively correlated with the average number of contacts between CS and PG (Figure 1i and Figure S3d, Supporting Information). This is mainly caused by: 1) The reduced number of hydrogen-bonded hydration water increased polymer chain flexibility; and 2) The increased number of hydrogen bonds between CS and PG facilitating the electro-interacting process (Figure S3d–f, Supporting Information). Consequently, under the same starting materials' concentration, increasing the temperature promotes the number of formed clusters (Figure 2j), leading to the formation of clusters with smaller sizes. The convergence of the simulation results delineated the difference in the synthesized CG NPs under different conditions, providing insights for the mechanism of CG formation.

## 2.2. Immunomodulatory Effects of $\beta$ -Glucan are Dependent on its Existing Form

The primary concerns for  $\beta$ -glucan based NPs are the immunoregulatory effects and the corresponding biosafety issue for potential in vivo studies. Contradictory results were proposed in previous studies, suggesting  $\beta$ -glucans could either stimulate pro-inflammatory effects,<sup>[7]</sup> or attenuate NLRP3 inflammasome

activation and subside I/R damage.<sup>[20]</sup> We hypothesize the immunostimulatory effects are both  $\beta$ -glucan concentration and existing form (water soluble  $\beta$ -glucan or particulate  $\beta$ -glucan) dependent.  $\beta$ -Glucan caused hyper-inflammation in phagocytes can be reflected by cellular viability decrease,<sup>[21]</sup> therefore we first tested whether water soluble PG and particulate CG had effects on the viability of monocytes/macrophages. Human monocytic (Mo) and phorbol 12-myristate 13-acetate (PMA) derived macrophages-like (M $\Phi$ ) THP-1 cells were incubated for 24 h with PG and CG at various concentrations. ATP-based luminescent assay showed negligible effects of PG and CG on the monocytes' viability compared with the phosphate-buffered saline (PBS) control at all concentrations, while only CG at high concentrations (> 100  $\mu$ g mL<sup>-1</sup>, in correspondence to PG concentration) induced lower cell viability (<90%) toward M $\Phi$  THP-1 cells (Figure S4a,b, Supporting Information). IL-1 $\beta$  excretion from Mo/M $\Phi$  THP-1 cells were in consistent with the viability study (Figure S4c,d, Supporting Information). Similar tendency was also observed in murine bone marrow derived macrophages (BMDMs), as reflected by the IL-1 $\beta$  secretion level (Figure S4e, Supporting Information); these suggest the stimulatory effects is less obvious from water soluble PG, but in a NP-concentration dependent manner for macrophages.

We hypothesize the inflammatory attenuation effect from  $\beta$ -glucans is caused by the immune memory from monocytes. Previous studies suggested  $\beta$ -glucan treated monocytes confer the sequentially derived macrophages protection against inflammatory challenges and retained NLRP3 inflammasome activation, which may account for its beneficial effects for I/R-induced cardiac damage.<sup>[20]</sup> In order to test whether this phenomenon is valid for our system, Mo THP-1 were pre-incubated with PG or CG at different concentrations for 24 h. Then the cell medium was removed and replaced by PMA-containing medium to obtain PMA-derived M $\Phi$  THP-1 cells, which were sequentially stimulated with lipopolysaccharide (LPS) and nigericin for canonical NLRP3 activation (Figure 2a). The cell viability was measured in M $\Phi$  THP-1 cells after NLRP3 inflammasome activation, and the results suggest that by pretreating Mo THP-1 cells with PG, but not CG, enhanced the M $\Phi$  THP-1 viability upon LPS/nigericin challenges in a PG concentration-dependent manner (Figure S4f, Supporting Information). This partly explains the inflammation attenuation effect from  $\beta$ -glucans as observed by previous reports.<sup>[20]</sup> Nonetheless, CG did not induce extra damage toward M $\Phi$  THP-1 cells upon NLRP3 activation at low concentration, despite failing in the inflammatory protection effect. Furthermore, as an inflammatory cell death indicator,<sup>[22]</sup> lactate dehydrogenase (LDH) release profiles were also measured, showing that only PG pretreatment reduced LDH release from M $\Phi$  THP-1 upon LPS/nigericin stimulation, whereas this was not observed for CG NPs, regardless of different concentrations (Figure 2b) and sizes (Figure 2c) tested.

BMDMs were used to measure the secretion of IL-1 $\beta$  and to analyze the immunomodulatory effects from PG and CG. Similarly, murine bone marrow derived monocytes were pre-incubated with PG or CG at different concentrations for 24 h, and the monocytes were further derived into BMDMs for further analysis (Figure S4g, Supporting Information). The pre-incubation of bone marrow monocytes with PG at higher concentration (50  $\mu$ g mL<sup>-1</sup>) reduced the amount of IL-1 $\beta$  found in the supernatant of BMDMs upon nigericin treatment. Pretreating

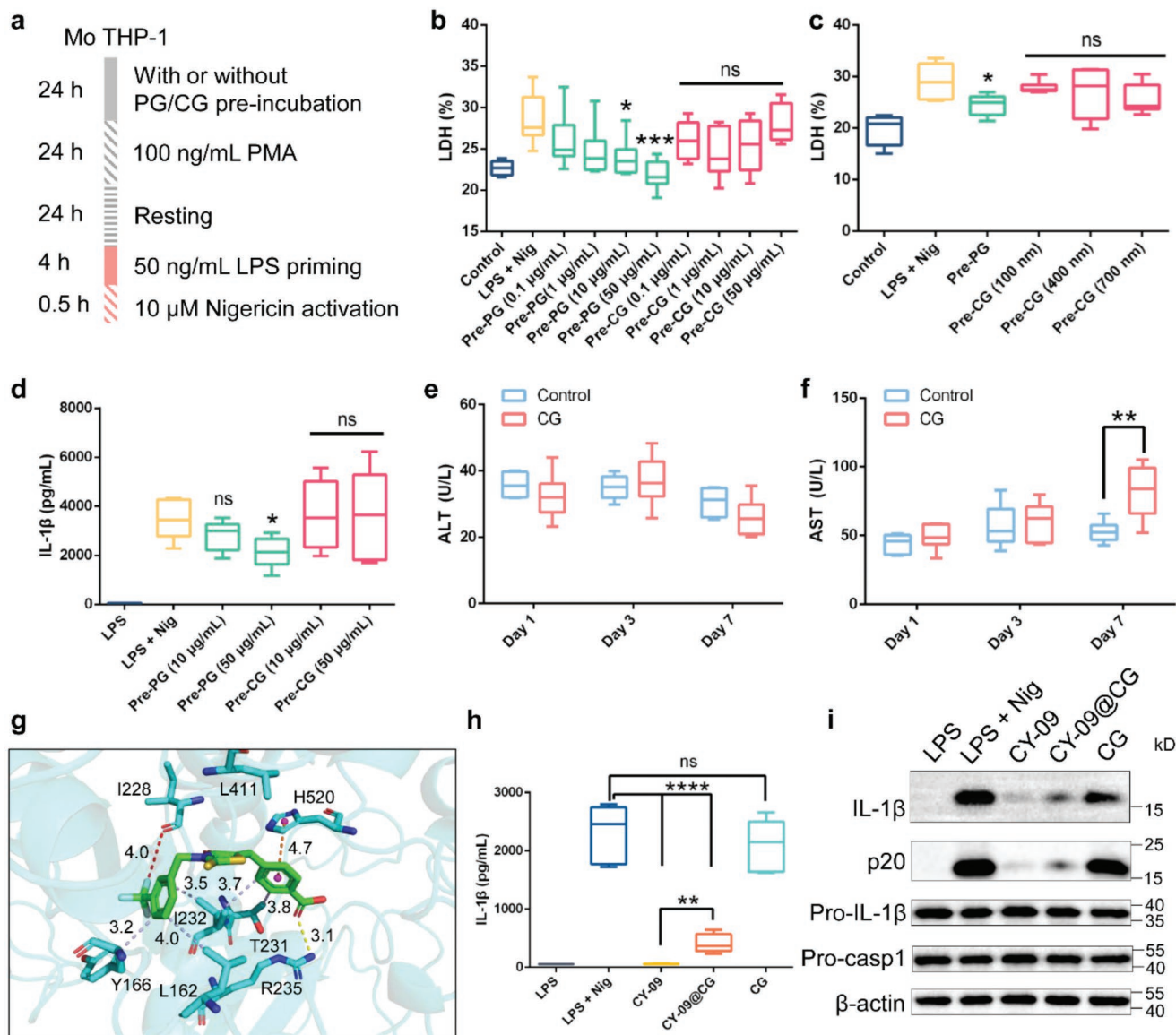


**Figure 2.** CY-09@CG effectively blocks NLRP3 activation in macrophages without stimulating extra inflammatory responses. a) Schematic overview for testing the effects of PG/CG on Mo THP-1 cells. Mo THP-1 cells were preincubated with PG or CG for 24 h. Then, the cells were differentiated into MΦ, sequentially challenged with canonical NLRP3 activation method (LPS+nigericin). b,c) LDH release after preincubating Mo THP-1 with PG induced a concentration dependent protection effect on MΦ THP-1 cells upon LPS+nigericin stimulation, whereas this phenomenon was not observed for CG regardless of concentrations (b) and sizes (c) tested. d) Preincubated mice bone marrow monocytes with PG, but not CG, reduced secretion of IL-1β upon LPS+nigericin stimulation of M-CSF-derived BMDMs. e,f) In vivo liver toxicity of CG NPs. C57BL/6 mice were i.v. injected with CG containing 8 mg kg<sup>-1</sup> PG for seven consecutive days. Serum ALT (e) and AST (f) levels were separately measured at day 1, 3, and 7. g) Docking complex and the potential interaction between NLRP3 and CY-09. Color indications: Cyan: NLRP3 (PDB: 6NPY); green: CY-09; red: halogen bond; yellow: salt bridge; orange: T-shape π-stacking; light-blue: hydrophobic interaction. The number indicates the bond length (unit: Å) whereas the letter + number indicates the serial number for the bond-forming amino acid. h) Production of IL-1β from BMDMs stimulated with LPS and nigericin and treated with CY-09 (10 μm), CY-09@CG (10 μm CY-09), or CG as measured by ELISA assay. i) Western blots of cell lysates (for evaluating Pro-IL-1β, Pro-casp-1, and β-actin) and supernatants (for evaluating IL-1β and p20) from BMDMs stimulated with LPS and nigericin and treated with CY-09 (10 μm), CY-09@CG (10 μm CY-09), or CG. Casp-1, caspase-1. Data in the graphs are shown as mean ± SD from six (b,c,e,f) or five (d,h) independent replicates. ns, no statistical significance; \**p* < 0.05, \*\**p* < 0.01, \*\*\**p* < 0.0005, and \*\*\*\**p* < 0.0001 compared with LPS + nigericin group (b–d) unless further specified (two-tailed Student's *t*-test).

monocytes with CG of different concentrations, albeit non-beneficial effects, did not induce extra IL-1β production comparing to LPS/nigericin group (Figure 2d). The above data demonstrate the inflammatory macrophages death is mainly observed in

particulate CG in a concentration-dependent manner. However, pretreatment of monocytes with water soluble PG, but not CG NPs, inhibiting the macrophages NLRP3 inflammasome activation. Concurrently, CG NPs did not induce extra damage to

both monocytic and M $\Phi$  cells at relatively low concentrations, suggesting their satisfied biosafety *in vitro*.

To access the biocompatibility of CG NPs for *in vivo* usages, liver toxicity assays were performed. CG was intravenously (*i.v.*) injected to healthy C57BL/6 mice at the PG concentration of 8 mg kg<sup>-1</sup> for seven-consecutive days, and the serum alanine transaminase (ALT) and the aspartate transaminase (AST) levels were monitored on days 1, 3, and 7 (Figure 2e,f). The administration of CG showed no effects on enhancing the serum ALT levels compared to the healthy control at all time-points tested, whilst long-term administration of CG (seven days) only slightly increased the serum levels of AST. Major organs were harvested after 1 month for hematoxylin and eosin (H&E) histopathological assessment, and no major difference was observed comparing to healthy mice (Figure S5, Supporting Information), suggesting that the administration of CG at low concentration is biocompatible and well-tolerated for short-term treatment strategy, such as inhibiting the NLRP3 inflammasomes for cardiac I/R post-conditioning.<sup>[23]</sup>

### 2.3. NLRP3 Inhibitor Loaded CG Suppressed Macrophage IL-1 $\beta$ Production

Next, CY-09, a specific NLRP3 inhibitor,<sup>[13]</sup> was further encapsulated in CG NPs (named CY-09@CG) to evaluate the degree of suppressed macrophages IL-1 $\beta$  production, which is the main downstream effector of NLRP3 inhibition.<sup>[14a]</sup> CY-09 was dispersed in the CS solution at the concentration of 0.1 mg mL<sup>-1</sup>, then the solution was filtered through 1.2  $\mu$ m membrane and further applied for constructing the CY-09@CG NPs. The encapsulation efficiency of CY-09 was determined to be 80.1%. The CY-09 releasing profile was also investigated for 24 h under sink conditions (PBS buffer, pH 7.4, containing 1% Poloxamer-407, Figure S6a, Supporting Information), and over 50% of the loaded CY-09 was released within the initial 4 h.

To investigate the NLRP3 inhibition efficiency and mechanism, we first simulated the binding mode of CY-09 to NLRP3 via homology modeling approach.<sup>[24]</sup> The protein-ligand complex crystal structure of NLRP3 kinase (PDB code: 6NPY) was chosen as the template and the binding site was defined as a cuboid. Docking of the compound CY-09 to the crystal structure of NLRP3 was performed using Autodock Vina and graphics were prepared by PyMOL.<sup>[24]</sup> The best conformation was observed when CY-09 docked into the ATP-binding pocket of NLRP3 kinase (Figure S6b, Supporting Information); the corresponding noncovalent interactions between proteins residues and CY-09 were obtained (Figure 2g), suggesting CY-09 may bind to the ATP-binding site in NACHT domain to inhibit NLRP3 ATPase and subsequent suppress NLRP3 oligomerization. This result provides insight on the mechanism of the potential molecular target of CY-09.

The biological effects of free CY-09 and CY-09@CG NPs on NLRP3 inflammasome activation were then tested in BMDMs, which were first primed with LPS, and then treated with different CY-09 formulations, and finally stimulated with nigericin.<sup>[22]</sup> IL-1 $\beta$  cytokine secretion was measured since it is required for the proteolytic processing by NLRP3 inflammasome to achieve the maximal production.<sup>[14a]</sup> The ELISA assay results did not detect obvious IL-1 $\beta$  secretion in the supernatant of BMDMs treated with LPS alone, whereas the release of IL-1 $\beta$  induced by nigericin

was blocked by both free CY-09 and CY-09@CG NPs (Figure 2h). The IL-1 $\beta$  level of CY-09@CG NPs was higher than CY-09 due to the release manner of CY-09 from the NPs (Figure 2h). Nonetheless, the LDH release profiles showed that CY-09 and CY-09@CG NPs have a similar effect on blocking the NLRP3-dependent pyroptotic cell death (Figure S6c, Supporting Information). Moreover, blank CG NPs did not lead to neither IL-1 $\beta$  nor LDH release from BMDMs, suggesting a good biocompatibility of the CG NPs. Immunoblot results (Figure 2i and Figure S6d, Supporting Information) showed that CY-09@CG NPs reduce the caspase-1 p20 (an auto-processed fragment of caspase-1) in cellular supernatant without affecting the expression of pro-caspase-1 in cellular lysates; this was also observed in a similar manner to free CY-09, suggesting that both CY-09 and CY-09@CG NPs inhibit the activation of caspase-1. As a downstream effect, the maturation of IL-1 $\beta$  was also inhibited by both CY-09 and CY-09@CG NPs, without affecting the expression of pro-IL-1 $\beta$ . The biological data are in good correspondence with the docking simulation, confirming the effective NLRP3 inhibition from CY-09@CG.

### 2.4. CG NPs Were Exclusively Recognized by Macrophages via Dectin-1

To demonstrate the Dectin-1 mediated unique selectivity of CG for Mo/M $\Phi$ , the interaction of fluorescently labeled CG (Fluor-CG, Figure S7a–c, Supporting Information) by Dectin-1 expressing Mo/M $\Phi$  THP-1 was evaluated by flow cytometry studies (Figure S8a, Supporting Information). For comparison, we applied  $\alpha$ -dextran, which shows no Dectin-1 binding capability,<sup>[9]</sup> for synthesizing phosphorylated dextran based NPs (termed as CD) in a similar manner, and further investigated its corresponding interaction with Dectin-1<sup>+</sup> Mo/M $\Phi$ . For Mo THP-1 cells, CG showed higher positive cell percentages but a marginal increased mean fluorescent intensity (MFI, Figure 3a; Figure S8b, Supporting Information), comparing to CD. However, for M $\Phi$  THP-1 cells, comparing to CD, CG showed less positive cell percentages, whereas a higher MFI (2.5-fold increase) was observed from positive cells subsets (Figure 3a and Figure S8c, Supporting Information). We hypothesize the mechanism for this phenomenon is due to the unique Dectin-1 mediated phagocytic pattern.<sup>[25]</sup> This is because Dectin-1 was shown to discriminate and phagocytize particulate  $\beta$ -glucans via a unique structure coined as “phagocytic synapse,” in which particulate  $\beta$ -glucans are recognized by Dectin-1, but phagocytized with the assistant from CD45 and CD148.<sup>[25]</sup> We confirmed that Mo THP-1 cells reached a 2-fold higher increase in the Dectin-1 expression comparing to M $\Phi$  THP-1 cells (Figure S8d,e, Supporting Information), suggesting that Mo THP-1 cells have better capability for recognizing  $\beta$ -glucans based NPs. In contrast, M $\Phi$  THP-1 cells showed a 2.8-fold CD45 expression and 2.7-fold CD148 expression compared to Mo THP-1 cells (Figure S8f–i, Supporting Information), suggesting that M $\Phi$  THP-1 cells have higher phagocytosis capability toward particulate  $\beta$ -glucans. Moreover, the CG binding/uptake efficiency by RAW 264.7 murine macrophages, which are known for low-to-no Dectin-1 expression,<sup>[26]</sup> was inferior to CD (Figure S8j–l, Supporting Information), suggesting that the cellular interactions with CG NPs might be mediated by Dectin-1.



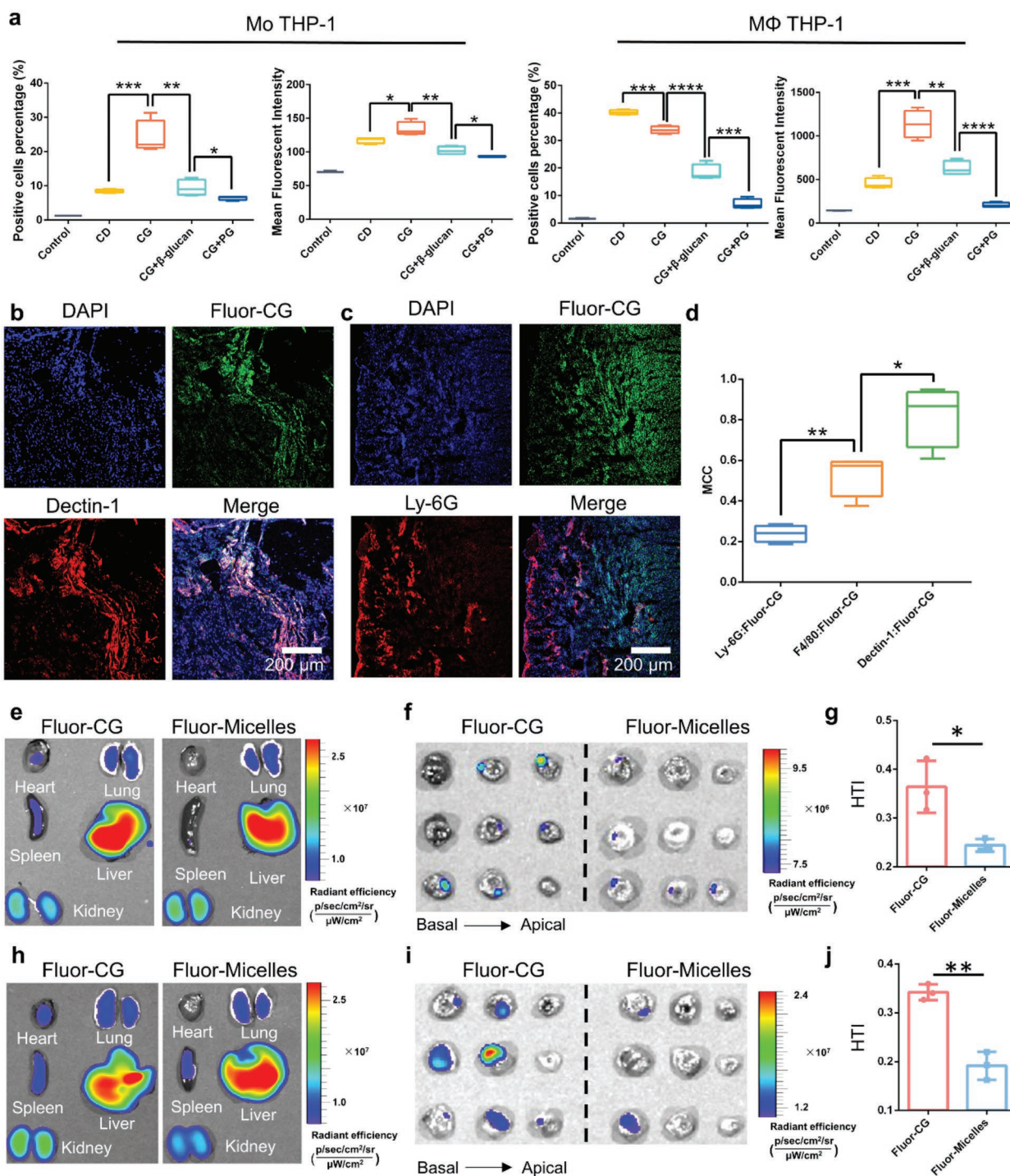


**Figure 3.** CG specifically targeted Dectin-1<sup>+</sup> Mo/MΦ, sequentially exhibiting an enhanced accumulation in the injured tissues after cardiac I/R. a) Cell uptake measurements demonstrate the propensity of the CG NPs to be specifically recognized and phagocytized via Dectin-1. Compared to  $\alpha$ -dextran-based NPs (CD), Dectin-1<sup>hi</sup>CD45<sup>low</sup>CD148<sup>low</sup> Mo THP-1 treated with Fluor-CG NPs showed higher positive cell percentages, while Dectin-1<sup>low</sup>CD45<sup>hi</sup>CD148<sup>hi</sup> MΦ THP-1 treated with Fluor-CG showed higher mean fluorescent intensity. Pristine barley  $\beta$ -glucan and PG blocked the interaction between CG and Mo/MΦ THP-1 cells. Representative dual-immunofluorescence staining of Fluor-CG and Ly-6G (b) or Fluor-CG and Dectin-1 (c) in murine heart at day 1 post-I/R, followed with quantitative analyses (d), confirming that CG NPs were mainly phagocytized by Dectin-1<sup>+</sup> macrophages. All scale bars indicate 200  $\mu$ m. Mapping of fluorescence to show the distribution of Fluor-CG and fluorescent dye dispersed into nano-micelles (Fluor-Micelles) in different organs at 24 h (e–g) and 48 h (h–j) post-I/R. Representative fluorescent mapping of Fluor-CG and Fluor-Micelles in major organs (e,h) as well as full data-set fluorescence accumulation in heart slices (f,i) are presented. HTI values quantitatively show the enhanced in vivo heart accumulation effect of Fluor-CG at both time-points (g,j). Values are expressed as the mean  $\pm$  SD of at least three independent trials. Statistical significance is assessed by two-tailed Student's *t*-test; \**p* < 0.05, \*\**p* < 0.01, \*\*\**p* < 0.0005 and \*\*\*\**p* < 0.0001.

Moreover, both addition of pristine barley  $\beta$ -glucan and PG blocked the interaction between the CG NPs and Mo/M $\Phi$  THP-1 cells, whereas this was not observed in RAW 264.7 macrophages (Figure 3a and Figure S8k,l, Supporting Information), confirming that the cellular interactions with CG NPs was mediated by Dectin-1. Notably, PG showed a higher blocking efficiency compared to pristine barley  $\beta$ -glucan, suggesting the increased Dectin-1 binding potential of barley  $\beta$ -glucan after phosphorylation (Figure 3a).

Overall, the corresponding surface marker differences explain the mechanism for the altered CG NPs uptake kinetics from different cell subsets, confirming the specific Dectin-1 mediated phagocytize pattern between CG NPs and Mo/M $\Phi$  cells.

## 2.5. CG NPs Targeted Dectin-1<sup>+</sup> Macrophages and Showed Increase Cardiac Accumulation after Myocardial I/R

In order to evaluate whether the Dectin-1<sup>+</sup> macrophages targeting strategy was feasible in vivo, confocal immunofluorescence microscopy of heart tissues were analyzed. Minimal macrophages signals (F4/80) but no Dectin-1 expression was observed in healthy murine hearts (Figure S9a, Supporting Information). C57BL/6 mice were surgically induced with ischemic damage by ligating left anterior descending artery (LAD, Movie S1, Supporting Information).<sup>[27]</sup> Obvious expression of Dectin-1 was observed at day 1 and 2 post-reperfusion (Figure S9b,c, Supporting Information), and Dectin-1 was mainly expressed in the infarcted and border areas of the infarcted tissue, with low-to-no expression in the non-infarct area of the heart (Figure S9d, Supporting Information). Neutrophils are also associated with massive IL-1 $\beta$  production and I/R-induced cardiac injury propagation.<sup>[6b]</sup> To identify the Dectin-1 expression and distribution on different leukocytes after cardiac I/R, and to clarify the current targeting strategy is specific for monocytes/macrophages, we conducted double-immunofluorescence staining of Dectin-1 together with F4/80 or Ly-6G. The results showed a major co-localization between Dectin-1 and F4/80 (Figure S9b,c, Supporting Information), but not between Dectin-1 and Ly-6G (Figure S9e, Supporting Information), as further quantitatively reflected by the Manders' colocalization coefficients (MCC, 0.58 vs 0.15,  $p = 0.005$ , Figure S9f, Supporting Information), suggesting Dectin-1 was mainly expressed on macrophages, but not on neutrophils after I/R-induced cardiac injury. Moreover, similar macrophages markers expression was rarely observed in murine heart from isoprenaline-induced cardiac hypertrophy model (Figure S9g, Supporting Information) and in human heart from late-stage heart failure (Figure S9h, Supporting Information), potentially suggesting the current targeting strategy may be exclusively suitable for myocardial I/R injury.

To further confirm the validation of the current targeting strategy for myocardial I/R, we investigated the potential cardiac accumulation of fluorescently labeled CG NPs (Fluor-CG). Fluor-CG NPs was i.v. injected at day 1 or day 2 post-I/R, and the heart was harvested at 1 h post-injection for fluorescent imaging. The heart of healthy mice showed no visible CG NPs accumulation (Figure S10a, Supporting Information), whereas the Fluor-CG NPs showed strong accumulation in infarcted

heart of mice at both day 1 (Figure 3b) and day 2 (Figure S10b, Supporting Information) post-I/R. Furthermore, the major co-localization was observed between Fluor-CG NPs and F4/80 (Figure S10b, Supporting Information), Fluor-CG NPs and Dectin-1 (Figure 3b), but less between Fluor-CG NPs and Ly-6G (Figure 3c), suggesting that the CG is mainly interacting with Dectin-1<sup>+</sup> macrophages but not neutrophils. The quantitative co-localization measurement confirmed that macrophages, but not neutrophils, mainly interacted with CG NPs (MCC, 0.53 vs 0.24,  $p = 0.002$ ). Nonetheless a more pronounced co-localization was observed between CG NPs and Dectin-1<sup>+</sup> subsets with the MCC of 0.82 ( $p = 0.018$ , vs Fluor-CG/F4/80, Figure 3g), suggesting the valid Dectin-1 targeting efficiency in vivo.

Mapping of the fluorescence in infarcted heart with an infrared fluorescent dye (Cyanine7, Cy7) showed the distribution of CG NPs. For this, the dye was either conjugated onto PG to form Fluor-CG NPs or dispersed in SolutolHS15 (Fluor-Micelles). In vivo biodistribution analysis was performed at one or two days post-I/R, and the major organs from mice were collected at 4 h post-i.v. injection (Figure S11a,b, Supporting Information). Comparing to Fluor-Micelles, a higher cardiac accumulation was observed from Fluor-CG NPs at both time-points. Fluorescent images of heart sections showed the major Fluor-CG accumulation was observed in left ventricular (LV) region, this is consistent with the aforementioned results that the Dectin-1<sup>+</sup> macrophages were mainly accumulated in the lesion sites of LV post-I/R (Figure 3d and Figure S9, Supporting Information). A quantitative analysis for comparing the cardiac accumulation of CG NPs was achieved by calculating the heart-targeting index (HTI; = average heart fluorescence emission/average liver fluorescence emission).<sup>[2c]</sup> A higher fluorescent signal from heart was observed from Fluor-CG group at both day 1 (49.2% enhancement) and day 2 (78.5% enhancement, Figure 3h).

Altogether, these results confirmed the valid Dectin-1 targeting capability of CG NPs in vivo, indicated the major NPs interaction with Dectin-1<sup>+</sup> macrophages, but not neutrophils, in infarcted area. The substantial recruited Dectin-1<sup>+</sup> macrophages sequester the CG NPs, which confer the propensity for CG accumulation in injured tissues, and thus, enhancing the cardiac accumulation of CG NPs post-I/R.

## 2.6. CY-09@CG NPs Attenuated I/R-Induced Myocardial Injury

We then evaluated the therapeutic effect of CY-09@CG and conventional CY-09 formulations (dispersed in FDA-approved solubilizer SolutolHS15 to form nano-micelles) on attenuating I/R-induced myocardial damage. CY-09 (0.5 mg kg<sup>-1</sup>), CY-09@CG or blank CG NPs were i.v. injected into mice at 10 min, 24 h, and 48 h post-I/R, the detailed schematic illustration of the treatment strategy was listed as Figure S12a, Supporting Information. The quantitative assessment of cardiac injury was first compared at 24 h after the reperfusion. The Evans blue/2, 3, 5-triphenyltetrazolium chloride (TTC) double staining results showed a similar size of areas at risk (AAR) in all experimental groups, indicating that the ligation was reproducibly performed at the same level of the left anterior coronary artery (Figure 4a,b).<sup>[7]</sup> Whereas comparing to model and CG group, the infarct area/AAR ratio was reduced

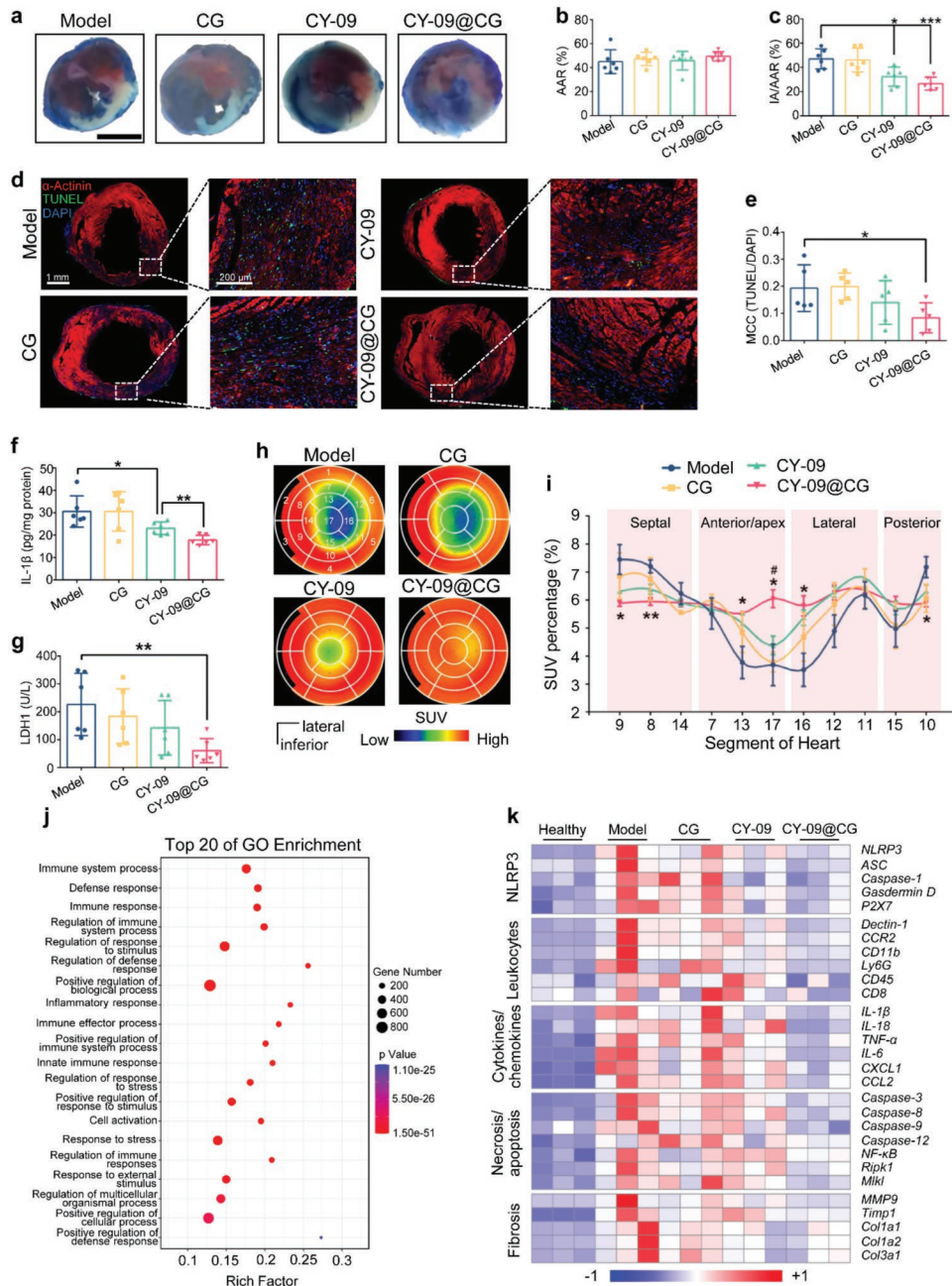


**Figure 4.** CY-09@CG better preserved I/R-induced cardiac damage through regulating innate immune responses. a) Representative photographs of heart sections from different groups stained with Evans blue and TTC staining at day 1 after I/R (scale bar, 2.5 mm). The images were further subjected for b) area at risk (AAR), and c) infarct area/AAR analysis ( $n = 6$ ). d) Representative photomicrographs of TUNEL (green) and nuclear (DAPI, blue) staining of cardiomyocytes ( $\alpha$ -Actinin, red) in infarct zone obtained from different groups at day 1 post-I/R ( $n = 5$ ). e) TUNEL-positive cells percentages were reflected as MCC between TUNEL and DAPI ( $n = 5$ ). f) Serological levels of LDH1 from different groups at 24 h post-I/R were further measured. g) Heart samples were obtained from different groups at 24 h post-I/R. Myocardial levels of IL-1 $\beta$  were assessed and compared with the whole protein amount. h) Representative LV seventeen-segment polar map reconstructed from the  $^{18}\text{F}$ -FDG PET imaging, and the i) quantitative analysis was evaluated via the percentage of SUV determined from PET imaging ( $n = 3$ ). j) The DEGs between CY-09@CG and Model groups were filtered for GO analysis ( $n = 3$ ), and the results suggested CY-09@CG-mediated biological processes were majorly enriched in immune responses. h) The gene expression of specific pathological signatures from I/R-induced cardiac injury, including proinflammatory (including NLRP3 inflammasome activation, leukocytes activation, and chemokine/cytokine production), necrosis/apoptosis, and profibrotic, were selected and generated into heat-map. Data are collected from biological independents. Statistical significance is assessed by two-tailed Student's  $t$ -test; data are shown as either mean  $\pm$  SD (b,c,e,f,g). \* $p < 0.05$ , \*\* $p < 0.01$ , \*\*\* $p < 0.0005$  or mean  $\pm$  SEM (i), \* $p < 0.05$ , \*\* $p < 0.01$  versus Model, # $p < 0.05$  versus CY-09. TTC, 2,3,5-triphenyltetrazolium chloride; TUNEL, terminal deoxynucleotidyl transferase-mediated deoxyuridinetriphosphate nick-end labeling; DAPI, 4',6-diamidino-2-phenylindole; MCC, Manders' colocalization coefficients; LDH1, lactate dehydrogenase 1;  $^{18}\text{F}$ -FDG, 8-fluoro-6-deoxyglucose; PET, positron emission tomography; SUV, standardized uptake value; DEGs, differentially expressed genes; GO, gene ontology.

after CY-09 treatment, and ratio was shown to be lower in the CY-09@CG NP group (26.7%,  $p = 0.0005$  vs Model) than in the CY-09 group (32.4%,  $p = 0.01$  vs Model, Figure 4c), albeit not statistically significant. Cardiac injury was also evaluated by terminal deoxynucleotidyl transferase mediated dUTP-biotin nick-end labeling (TUNEL) and  $\alpha$ -actinin (cardiomyocytes marker) staining (Figure 4d). CY-09 and CY-09@CG treatment decreased the number of TUNEL<sup>+</sup> cells and preserved  $\alpha$ -Actinin<sup>+</sup> cardiomyocytes (Figure 4e and Figure S12b, Supporting Information), whereas the statistical significance was solely observed from CY-09@CG group, suggesting a better treatment efficacy from CY-09@CG. This is consistent with the serological analysis at 24 h post-I/R, where the cardiomyocytes markers creatine kinase myocardial band (CK-MB) was reduced by 51.2% ( $p = 0.009$ ) from CY-09@CG treatment (Figure S12c, Supporting Information). To test whether CY-09@CG obtains better efficiency in blocking the overall cardiac NLRP3 inflammasome activation, we also assessed the protein levels of IL-1 $\beta$  in the myocardium. The IL-1 $\beta$  decreased by 37% with CY-09 treatment, whereas the cardiac IL-1 $\beta$  production was further reduced by 62% through CY-09@CG treatment ( $p = 0.0043$ , vs CY-09, Figure 4f), similarly, serological level of lactate dehydrogenase 1 (LDH1), as an indicator for cardiomyocytes pyroptosis,<sup>[22,28]</sup> from Model group was higher compared with CY-09@CG group ( $p = 0.007$ ), but not to CY-09 group (Figure 4g). These results confirmed that comparing to the conventional nano-micelles formulation of CY-09, CY-09@CG could better remit I/R-induced cardiomyocytes death, and the protective effect from CY-09@CG may be partly attributable to the inhibitory effects for NLRP3 inflammasome.

To assess whether the therapeutic effects may ameliorate the cardiac metabolism, we next conducted positron emission tomography-computed tomography (PET-CT) at 48 h post-I/R.<sup>[28]</sup> Seventeen-segment polar map (Figure S13, Supporting Information) were further generated based on the PET-CT images (Figure S14 and Movies S2–S5, Supporting Information) to quantitatively assess the LV metabolism through the percentage of standardized uptake value (SUV) of 8-fluoro-6-deoxyglucose (<sup>18</sup>F-FDG, Figure 4h).<sup>[28]</sup> CY-09@CG better preserved the apex (Segment 17, S17) and apical anterior/lateral (S13, S16) cardiomyocytes after I/R stress. Notably, SUV percentage of mid-anteroseptal (S8), mid-inferoseptal (S9), mid-posterior (S10) segments from CY-09@CG group were lower than those from Model group, whereas CY-09 fail to mount a statistical difference, indicating CY-09@CG attenuated the compensatory metabolism in antero/infero-septal LV region (Figure 4i).

To better identify genetic networks underlying I/R process, and to gain a deeper understanding of potential mechanisms of therapeutic response to CY-09@CG, we performed RNA sequencing (RNA-seq) in LV samples from different groups at 24 h post-I/R. The detailed description for filtering differentially expressed genes (DEGs) were described in Supporting Information (SI), and gene ontology (GO) enrichment of biological process terms and Kyoto Encyclopedia of Genes and Genomes (KEGG) pathway analysis were performed with different DEGs. Comparing to healthy control, 2289 genes were highly expressed in left ventricular tissue after I/R process (Figure S15a, Supporting Information), and KEGG pathway analysis showed major enrichment of these genes in

chemokine signaling pathway, cytokine-cytokine receptor interaction, leukocytes transendothelial migration, etc. (Figure S15b, Supporting Information). This is consistent with the GO analysis on biological process (Figure S15c, Supporting Information), suggesting the major participation of inflammation in I/R-induced myocardial injury. Of note, Gene Set Enrichment Analysis (GSEA) suggesting the Model and treatment groups exhibited similar reperfusion condition (Figure S15d,e, Supporting Information), whereas over 87% of the up-regulated DEGs provoked by I/R process are subsided by CY-09@CG treatment (Figure S15f, Supporting Information). We further filtered out the DEGs between Model and CY-09@CG group by different methods,<sup>[28,29]</sup> and the majority of top GO and KEGG pathway enrichments were annotated as stress/immune responses (Figure 4j; Figure S15g,h, Supporting Information), suggesting CY-09@CG treatment induced transcriptional regulation were tightly associated with a reduction in inflammation.

We further plotted the expression of pathological indicators induced by I/R process to profile the effects from CY-09@CG (Figure 4k). Comparing to the nano-micelles formulation of CY-09, CY-09@CG showed almost complete abrogation of pathological RNA expression signatures induced by I/R-induced myocardial injury. Upregulation of proinflammatory (including NLRP3 activation, leukocytes infiltration/activation, chemokine/cytokine production) and apoptosis/necrosis genes were attenuated by CY-09@CG with better efficiency. Meanwhile, the pro-fibrotic process, which is highly correlated with the inflammatory condition, was also re-established. Overall, the results highlighted the functional significance of suppressing NLRP3 inflammasome activation in mediating cardiac injury after I/R process. Moreover, these results are consistent with the concept that specific inhibiting Dectin-1<sup>+</sup> macrophages NLRP3 inflammasome via CY-09@CG obtains superior therapeutic efficiency comparing to conventional nano-micelles based formulation.

## 2.7. CY-09@CG NPs Ameliorate Long-Term Prognosis after Cardiac I/R

To determine the translational potential of such strategy, we evaluated the long-term prognosis after the treatment. We first measured the ejection fraction (EF), fractional shortening (FS), LV end-diastolic volume (LVEDV), LV end-systolic volume (LVESV), LV internal diameter at end-diastole (LVID, d), and LV internal diameter at end-systole (LVID, s) with echocardiograph (ECG) at one and five weeks after I/R (Table S1, Supporting Information). At one week follow-up, despite no difference in LVEDV was observed between Model, CG, CY-09 and CY-09@CG groups (Figure 5a,b), I/R-induced cardiac contractile dysfunction (as indicated by decreases in EF and FS, and the enhancement in LVEDV) was attenuated by both CY-09 and CY-09@CG treatment (Figure S16a, Supporting Information), where CY-09@CG showed a higher EF and FS than CY-09 group. Sequentially, the preserved cardiac function by CY-09@CG was confirmed by the enhanced EF and FS, as well as the reduced LVEDV and LVESV (Figure 5c,d and Figure S16b, Supporting Information), whereas this phenomenon is non-significant from CY-09 group. Moreover, CY-09@CG treatment, but

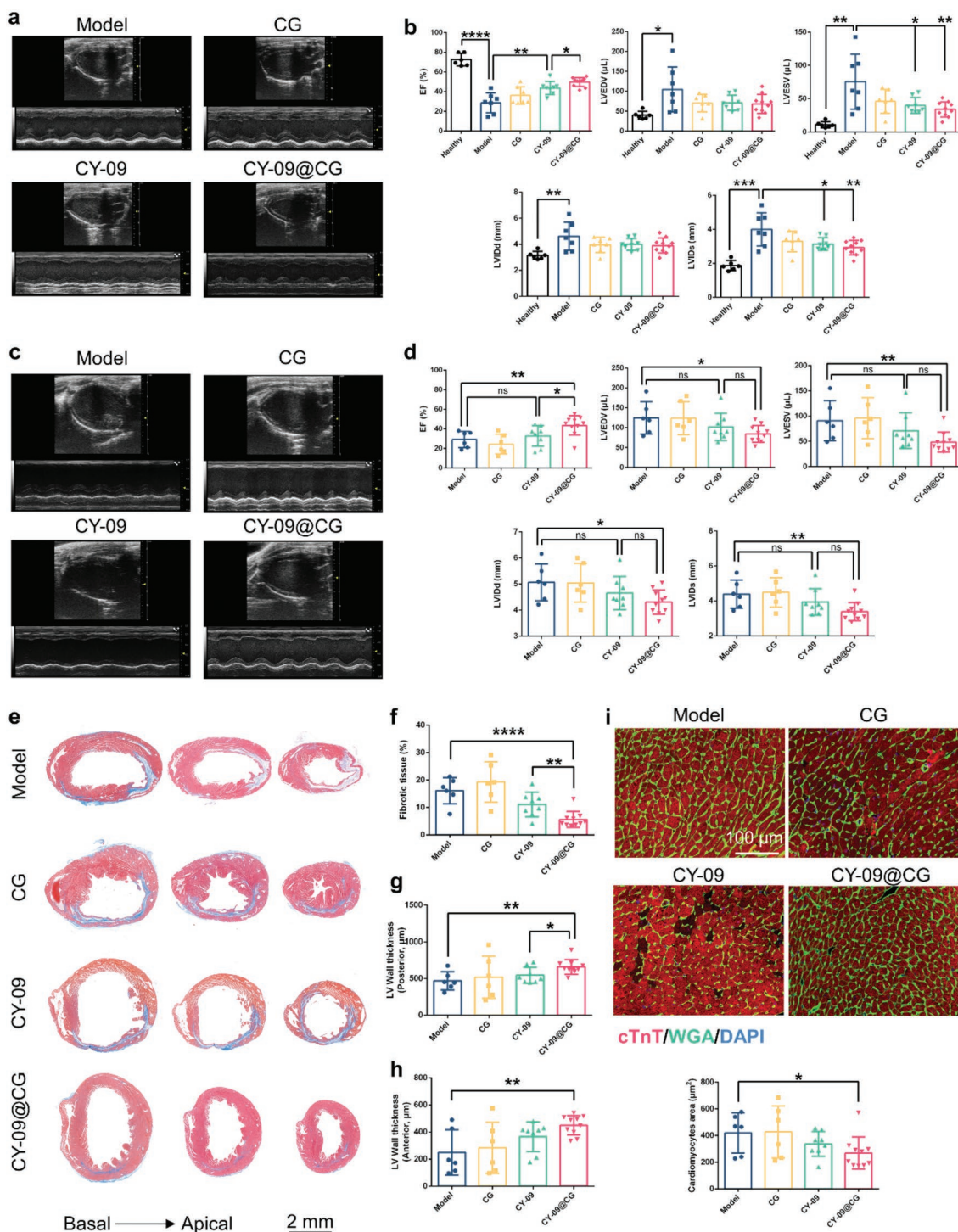


**Figure 5.** CY-09@CG showed better efficiency in ameliorating long-term prognosis after I/R cardiac injury. Representative M-mode echocardiographic images in different groups of mice at 1 week (a) or 5 weeks (c) post-I/R, and the corresponding quantitative evaluation of EF, FS, LVEDV, LVESV, LVID, d and LVID, s at 1 week (b) or 5 weeks (d) follow up were sequentially determined. e) Representative Masson's trichrome-stained sections of hearts harvested at 5 weeks post-I/R (bar = 2 mm). f) Fibrotic tissue percentage measured at 5 weeks post-I/R in Masson's trichrome stained tissue sections ( $n = 6-10$ ). LV wall thickness of the g) posterior and h) anterior myocardium measured in Masson's trichrome-stained tissue sections at 5 weeks post-I/R ( $n = 6-10$ ). i) Representative staining with WGA (green), cTnT (red), and DAPI (blue) to visualize cardiomyocytes in sections from the remote area and the corresponding quantification of cross-sectional surface area of cardiomyocytes, as assessed by WGA staining ( $n = 6-10$ ). Data are shown as mean  $\pm$  SD; statistical significance is assessed by two-tailed Student's *t*-test; \* $p < 0.05$ , \*\* $p < 0.01$ , \*\*\*\* $p < 0.0001$ . EF, ejection fraction; LVEDV, left ventricular end-diastolic volume; LVESV, left ventricular end-systolic volume; LVID, d, left ventricular end-diastolic inner diameter; LVID, s, left ventricular end-systolic inner diameter; LV, left ventricular; cTnT, cardiac troponin T; WGA, wheat germ agglutinin; DAPI, 4',6-diamidino-2-phenylindole.

not CY-09, remarkably restricted LV dilation, as assessed by LVID, d and LVID, s, comparing to the Model group. Fibrosis critically determines the prognosis of I/R-induced cardiac injury,<sup>[30]</sup> and Masson's trichrome staining at five weeks follow-up showed a decrease in the area of detectable fibrotic tissue after the CY-09@CG NPs treatment within a comparable relative fibrotic tissue length (Figure 5e,f and Figure S16c, Supporting Information). In contrast, CY-09 group showed a less striking amelioration efficiency. Consistently, histology images indicated an increase in LV anterior/posterior wall thickness solely from CY-09@CG group (Figure 5g,h and Figure S16d, Supporting Information). The ameliorated fibrosis level also remitted the hypertrophy of survival cardiomyocytes, as confirmed by the reduced cross-sectional area of cardiomyocytes (located in remote area) from CY-09@CG group, whereas CY-09 were unable to mount a significant attenuation (Figure 5i), suggesting that comparing to conventional CY-09 nano-micelles, CY-09@CG NPs protected the heart from I/R-induced alterations in cardiac morphology with better efficiency. In summary, these results demonstrate a proof-of-concept that therapeutic targeting of Dectin-1<sup>+</sup> macrophages via  $\beta$ -glucan NPs is a promising strategy for cardiac I/R post-conditioning and future clinical translation.

### 3. Conclusion

Harnessing the intense inflammatory response is revolutionizing the treatment strategies of I/R injury, yet the off-target immunosuppressant may damage the homeostasis and lead to side effects, therefore the clinical translation of the corresponding therapies is usually precluded by the lack of drug selectivity toward specific cellular subsets or signaling pathway.<sup>[6]</sup> For example, although preclinical studies suggested pharmacological inhibition of NLRP3 inflammasome activation ameliorates I/R-induced myocardial injury,<sup>[31]</sup> systematic NLRP3 deficiency conversely increased infarct size,<sup>[32]</sup> suggesting the benefits from NLRP3 inhibition for I/R damage may be cell-type-dependent and time-dependent.<sup>[14b,33]</sup> Hence a targeted treatment might further amplify the therapeutic outcome.

Conventional targeting ligand functionalization usually involves trivial modification process, and the potentially subsided targeting yield in vivo also hinders their translational perspective.<sup>[4]</sup> Therefore, targeting-ligand free NPs with inherent targeting capability is preferred. To achieve this, two fundamental questions were concomitantly proposed: 1) Which materials should be chosen to fabricate the NPs; and 2) how to develop an economically feasible nanosystem in a simple and robust manner, which are important factors for potential translation into clinical practice.

Herein, we applied a natural Dectin-1 ligand,  $\beta$ -glucan, as starting material for fabricating NPs to avoid any surface modification of the NPs.<sup>[9]</sup> A modified modular microfluidic platform facilitated the single step production of  $\approx$ 100 nm of  $\beta$ -glucan based NPs (CG NPs) in a continuous and reproducible manner. Comparing to conventional  $\beta$ -glucan NPs fabrication method, such as metal immobilization or thermal denaturation,<sup>[11]</sup> CG NPs show advantages in simple producing procedure,

long-term stability, and high drug loading degree. Accompanied with in silico mechanistic interpretation of CG NPs formation, these data might facilitate the translation of current nanosystem into a wider pharmaceutical practice.

Biosafety and biocompatibility are the pre-requisite of drug vehicles, yet a paradox role of  $\beta$ -glucan was purposed by previous studies, suggesting it can be either immunoprotective or immunostimulative.<sup>[7,20]</sup> Our results proved water soluble  $\beta$ -glucan (PG) can induce macrophage-protection effects toward inflammatory challenges, whereas the immunostimulatory effects were mainly observed in particulate  $\beta$ -glucan (CG NPs) at high concentrations. These findings provide potential explanation for the discrepant biological effects of  $\beta$ -glucan observed by previous researches. Despite the non-salutary effects from CG NPs, we confirmed the biocompatibility and feasibility of CG NPs for cardiac I/R treatment, as reflected by the in vivo liver toxicity and long-term histochemical analysis after NP-administration.

Precise Dectin-1 targeting efficiency of CG NPs was confirmed both in vitro and in vivo. The recognition of CG NPs by monocytes/macrophages was dictated by Dectin-1, whereas the phagocytosis was co-governed by CD45 and CD148, this cellular interaction pattern is uniquely observed in Dectin-1 mediated phagocytosis but no other innate PRRs,<sup>[25]</sup> implying precise Dectin-1 targeting capability of CG NPs. Among other leukocytes, the highest MCC was observed between Dectin-1<sup>+</sup> macrophages and CG NPs, suggesting the Dectin-1 targeting capability from CG NPs was also valid in vivo after cardiac I/R. Moreover, we confirmed the expression of Dectin-1 in human heart from other cardiac diseases, potentially suggesting the currently purposed strategy may also suitable for a wider clinical scenario beyond myocardial reperfusion injury.

The NLRP3 inhibition efficiency from CY-09@CG NPs was confirmed in silico, in vitro, and in vivo. In both acute and chronic I/R settings, CY-09@CG outperformed the conventional CY-09 formulation, nano-micelles prepared by FDA-approved solubilizer SolutolHS15, in restraining the infarct size, reducing the myocardial NLRP3 inflammasome activity, preserving the cardiac functions and ameliorating the long-term prognosis. Previous studies focused on NLRP3 induced direct pyroptosis of cardiac parenchyma cells,<sup>[14b,23]</sup> whereas the systematic investigation on specifically inhibiting monocytes/macrophages NLRP3, albeit their capability in indirectly promote the injury, is relatively less. Herein, RNA-seq analysis revealed that, besides of directly regulating inflammatory responses, specific Dectin-1<sup>+</sup> monocytes/macrophages NLRP3 inhibition also subsided the necrosis, apoptosis, and fibrosis, which are critical pathological indicators for I/R-induced myocardial damage. This observation underscores the functional significance of Dectin-1<sup>+</sup> monocytes/macrophages as major mediator for genesis and propagation of I/R-induced cardiac injury.<sup>[7,34]</sup> Noteworthy, in the chronic I/R setting (five weeks post-I/R), the beneficiary effects from free CY-09 was nearly abolished, whereas CY-09@CG can still mount a significant cardiac injury amelioration. As recently purposed, intra-cardiac administrated  $\beta$ -glucan (zymosan) will persist in heart, and have an important role in the later stages (after three days) of infarct maturation and recovery, which are hypothesized mainly by modulating

the Cx3cr1<sup>+</sup>Ccr2<sup>+</sup> monocytes extravasation.<sup>[35]</sup> Different from previous works,<sup>[7,34]</sup> we tested the concept of selective inhibition of critical signaling pathway in Dectin-1<sup>+</sup> macrophages, rather than simply depletion or antibody-mediated neutralization, in attenuating I/R stress in preclinical models. This new method may avoid the severe side effects due to systematic Dectin-1 deficiency,<sup>[8]</sup> thus provide potential “targeting framework” for I/R injury treatment.

In summary, as proof-of-concept, we showed that specific NLRP3 inflammasome inhibition in Dectin-1<sup>+</sup> macrophages ameliorated I/R-induced cardiac damage and better preserved the cardiac function in vivo. The developed  $\beta$ -glucan NPs can be further applied to multiple inflammatory-related diseases due to its specific targeting capability toward Dectin-1<sup>+</sup> macrophages, and we expect that the simple and modular production method of this  $\beta$ -glucan NPs can pave the way for facilitating its clinical translation.

## 4. Experimental Section

The detailed description of methods is listed in Supporting Information. All experiments involving animals were performed in compliance with the guidelines from and were approved by the Institutional Animal Care and Use Committee of Ruijin Hospital, Shanghai Jiao Tong University School of Medicine and Institutional Animal Care and Use Committee of Experimental Animal Centre in Xiamen University, China.

## Supporting Information

Supporting Information is available from the Wiley Online Library or from the author.

## Acknowledgements

Z.L., W.L., and Q.L. contributed equally to this work. This work was supported by grants from the National Key R&D Program and the National Natural Science Foundation of China (Nos. 2017YFA0504504, 22025702, 91853203 and 82021003), the Fundamental Research Funds for the Central Universities of China (Nos. 20720190101 and 20720200008), the Program of Introducing Talents of Discipline to Universities (B06016), the National Science Foundation for Distinguished Young Scholar of China (No. 8212500418), the Academy of Finland (Nos. 317042, 340129, and 331151), the Orion Research Foundation, the Sigrid Jusélius Foundation, and the UMG Research Funds. The authors acknowledge the support from Dr. Wangxi Hai (Department of Nuclear Medicine, Ruijin Hospital, China), Dr. Wenchang Xiao (Raydata Technology Co., China), Dr. Xiangwei Wu (igeneCode Biotech Co., China), and Dr. Mei Gao (Institute of Translational Medicine, Shanghai Jiaotong University, China) in analyzing the data. The authors acknowledge the support from Biorender in art design, Magnus Ehrnrooth Foundation, Ölvi Foundation (No. 2020032), Väre children cancer Foundation, Finnish-Norwegian medical Foundation, Tor, Joe and Pentti Borg Foundation, Ida Montin Foundation and Waldemar Von Frenckell Foundation. The authors also acknowledge the computational resources of the Finnish IT Centre for Scientific Computing (CSC).

## Conflict of Interest

The authors declare no conflict of interest.

## Data Availability Statement

The data that support the findings of this study are available from the corresponding author upon reasonable request.

## Keywords

$\beta$ -glucan, Dectin-1, microfluidics, myocardial reperfusion, NLRP3 inflammasomes

Received: April 25, 2022

Revised: May 18, 2022

Published online: June 29, 2022

- [1] S. Kaptoge, L. Pennells, D. De Bacquer, M. T. Cooney, M. Kavousi, G. Stevens, L. M. Riley, S. Savin, T. Khan, S. Altay, P. Amouyel, G. Assmann, S. Bell, Y. Ben-Shlomo, L. Berkman, J. W. Beulens, C. Björkelund, M. Blaha, D. G. Blazer, T. Bolton, R. Bonita Beaglehole, H. Brenner, E. J. Brunner, E. Casiglia, P. Chamnan, Y.-H. Choi, R. Chowdry, S. Coady, C. J. Crespo, et al., *Lancet Glob. Health* **2019**, *7*, e1332.
- [2] a) A. M. Flores, N. Hosseini-Nassab, K.-U. Jarr, J. Ye, X. Zhu, R. Wirka, A. L. Koh, P. Tsantilas, Y. Wang, V. Nanda, Y. Kojima, Y. Zeng, M. Lotfi, R. Sinclair, I. L. Weissman, E. Ingelsson, B. R. Smith, N. J. Leeper, *Nat. Nanotechnol.* **2020**, *15*, 154; b) Z. Liu, Y. Li, W. Li, C. Xiao, D. Liu, C. Dong, M. Zhang, E. Mäkilä, M. Kemell, J. Salonen, J. T. Hirvonen, H. Zhang, D. Zhou, X. Deng, H. A. Santos, *Adv. Mater.* **2018**, *30*, 1703393; c) M. Shin, H.-A. Lee, M. Lee, Y. Shin, J.-J. Song, S.-W. Kang, D.-H. Nam, E. J. Jeon, M. Cho, M. Do, S. Park, M. S. Lee, J.-H. Jang, S.-W. Cho, K.-S. Kim, H. Lee, *Nat. Biomed. Eng.* **2018**, *2*, 304.
- [3] a) R. Brusini, M. Varna, P. Couvreur, *Adv. Drug Delivery Rev.* **2020**, *157*, 161; b) G. Torrieri, F. Fontana, P. Figueiredo, Z. Liu, M. P. A. Ferreira, V. Talman, J. P. Martins, M. Fusciello, K. Moslova, T. Teesalu, V. Cerullo, J. Hirvonen, H. Ruskoaho, V. Balasubramanian, H. A. Santos, *Nanoscale* **2020**, *12*, 2350; c) M. P. A. Ferreira, V. Talman, G. Torrieri, D. Liu, G. Marques, K. Moslova, Z. Liu, J. F. Pinto, J. Hirvonen, H. Ruskoaho, H. A. Santos, *Adv. Funct. Mater.* **2018**, *28*, 1705134.
- [4] V. Mirshafiee, M. Mahmoudi, K. Lou, J. Cheng, M. L. Kraft, *Chem. Commun.* **2013**, *49*, 2557.
- [5] V. Balasubramanian, Z. Liu, J. Hirvonen, H. A. Santos, *Adv. Healthcare Mater.* **2018**, *7*, 1700432.
- [6] a) R. Duivenvoorden, M. L. Senders, M. M. T. van Leent, C. Pérez-Medina, M. Nahrendorf, Z. A. Fayad, W. J. M. Mulder, *Nat. Rev. Cardiol.* **2019**, *16*, 21; b) F. K. Swirski, M. Nahrendorf, *Nat. Rev. Immunol.* **2018**, *18*, 733.
- [7] Q. Fan, R. Tao, H. Zhang, H. Xie, L. Lu, T. Wang, M. Su, J. Hu, Q. Zhang, Q. Chen, Y. Iwakura, W. Shen, R. Zhang, X. Yan, *Circulation* **2019**, *139*, 663.
- [8] I. D. Iliev, V. A. Funari, K. D. Taylor, Q. Nguyen, C. N. Reyes, S. P. Strom, J. Brown, C. A. Becker, P. R. Fleshner, M. Dubinsky, J. I. Rotter, H. L. Wang, D. P. B. McGovern, G. D. Brown, D. M. Underhill, *Science* **2012**, *336*, 1314.
- [9] G. D. Brown, S. Gordon, *Nature* **2001**, *413*, 36.
- [10] a) M. Aouadi, G. J. Tesz, S. M. Nicoloso, M. Wang, M. Chouinard, E. Soto, G. R. Ostroff, M. P. Czech, *Nature* **2009**, *458*, 1180; b) L. D. Halder, E. A. H. Jo, M. Z. Hasan, M. Ferreira-Gomes, T. Krüger, M. Westermann, D. I. Palme, G. Rambach, N. Beyersdorf, C. Speth, I. D. Jacobsen, O. Kniemeyer, B. Jungnickel, P. F. Zipfel, C. Skerka, *Nat. Commun.* **2020**, *11*, 2331.

- [11] a) R. S. Singh, N. Kaur, J. F. Kennedy, *Carbohydr. Polym.* **2015**, *123*, 190; b) X. Jia, Q. Liu, S. Zou, X. Xu, L. Zhang, *Carbohydr. Polym.* **2015**, *117*, 434.
- [12] a) D. Liu, S. Cito, Y. Zhang, C.-F. Wang, T. M. Sikanen, H. A. Santos, *Adv. Mater.* **2015**, *27*, 2298; b) I. Arduino, Z. Liu, A. Rahikkala, P. Figueiredo, A. Correia, A. Cutrignelli, N. Denora, H. A. Santos, *Acta Biomater.* **2020**, *121*, 566.
- [13] H. Jiang, H. He, Y. Chen, W. Huang, J. Cheng, J. Ye, A. Wang, J. Tao, C. Wang, Q. Liu, T. Jin, W. Jiang, X. Deng, R. Zhou, *J. Exp. Med.* **2017**, *214*, 3219.
- [14] a) K. V. Swanson, M. Deng, J. P. Y. Ting, *Nat. Rev. Immunol.* **2019**, *19*, 477; b) E. Mezzaroma, S. Toldo, D. Farkas, I. M. Seropian, B. W. Van Tassell, F. N. Salloum, H. R. Kannan, A. C. Menna, N. F. Voelkel, A. Abbate, *Proc. Natl. Acad. Sci. USA* **2011**, *108*, 19725; c) Y. Liu, K. Lian, L. Zhang, R. Wang, F. Yi, C. Gao, C. Xin, D. Zhu, Y. Li, W. Yan, *Basic Res. Cardiol.* **2014**, *109*, 415; d) Ø. Sandanger, T. Ranheim, L. E. Vinge, M. Bliksøen, K. Alfsnes, A. V. Finsen, C. P. Dahl, E. T. Askevold, G. Florholmen, G. Christensen, K. A. Fitzgerald, E. Lien, G. Valen, T. Espevik, P. Aukrust, A. Yndestad, *Cardiovasc. Res.* **2013**, *99*, 164; e) S. I. Gringhuis, T. M. Kaptein, B. A. Wevers, B. Theelen, M. van der Vlist, T. Boekhout, T. B. H. Geijtenbeek, *Nat. Immunol.* **2012**, *13*, 246; f) S. I. Gringhuis, J. den Dunnen, M. Litjens, M. van der Vlist, B. Wevers, S. C. M. Bruijns, T. B. H. Geijtenbeek, *Nat. Immunol.* **2009**, *10*, 203.
- [15] a) M. Mahmoudi, M. Yu, V. Serpooshan, J. C. Wu, R. Langer, R. T. Lee, J. M. Karp, O. C. Farokhzad, *Nat. Nanotechnol.* **2017**, *12*, 845; b) C. D. Walkey, J. B. Olsen, H. Guo, A. Emili, W. C. W. Chan, *J. Am. Chem. Soc.* **2012**, *134*, 2139.
- [16] T. Sato, J. Nishimura-Uemura, T. Shimosato, Y. Kawai, H. Kitazawa, T. Saito, *J. Food Prot.* **2004**, *67*, 1719.
- [17] Z. Liu, F. Fontana, A. Python, J. T. Hirvonen, H. A. Santos, *Small* **2020**, *16*, 1904673.
- [18] Z. Liu, Y. Li, W. Li, W. Lian, M. Kemell, S. Hietala, P. Figueiredo, L. Li, E. Mäkilä, M. Ma, J. Salonen, J. T. Hirvonen, D. Liu, H. Zhang, X. Deng, H. A. Santos, *Mater. Horiz.* **2019**, *6*, 385.
- [19] P. Garstecki, M. A. Fischbach, G. M. Whitesides, *Appl. Phys. Lett.* **2005**, *86*, 244108.
- [20] a) G. Camilli, M. Bohm, A. C. Piffer, R. Lavenir, D. L. Williams, B. Neven, G. Grateau, S. Georgin-Lavialle, J. Quintin, *J. Clin. Invest.* **2020**, *130*, 4561; b) C. Li, T. Ha, J. Kelley, X. Gao, Y. Qiu, R. L. Kao, W. Browder, D. L. Williams, *Cardiovasc. Res.* **2004**, *61*, 538.
- [21] a) M. G. Schäppi, C. Deffert, L. Fiette, G. Gavazzi, F. R. Herrmann, D. C. Belli, K. H. Krause, *J. Pathol.* **2008**, *214*, 434; b) I. Tabas, *Nat. Rev. Immunol.* **2010**, *10*, 36.
- [22] R. C. Coll, A. A. B. Robertson, J. J. Chae, S. C. Higgins, R. Muñoz-Planillo, M. C. Inserra, I. Vetter, L. S. Dungan, B. G. Monks, A. Stutz, D. E. Coker, M. S. Butler, M. Haneklaus, C. E. Sutton, G. Núñez, E. Latz, D. L. Kastner, K. H. G. Mills, S. L. Masters, K. Schroder, M. A. Cooper, L. A. J. O'Neill, *Nat. Med.* **2015**, *21*, 248.
- [23] S. Toldo, A. Abbate, *Nat. Rev. Cardiol.* **2018**, *15*, 203.
- [24] O. Trott, A. J. Olson, *J. Comput. Chem.* **2010**, *31*, 455.
- [25] H. S. Goodridge, C. N. Reyes, C. A. Becker, T. R. Katsumoto, J. Ma, A. J. Wolf, N. Bose, A. S. H. Chan, A. S. Magee, M. E. Danielson, A. Weiss, J. P. Vasilakos, D. M. Underhill, *Nature* **2011**, *472*, 471.
- [26] G. D. Brown, J. Herre, D. L. Williams, J. A. Willment, A. S. J. Marshall, S. Gordon, *J. Exp. Med.* **2003**, *197*, 1119.
- [27] K. Reichert, B. Colantuono, I. McCormack, F. Rodrigues, V. Pavlov, M. R. Abid, *JoVE* **2017**, e55353.
- [28] S. Huang, D. Lei, Q. Yang, Y. Yang, C. Jiang, H. Shi, B. Qian, Q. Long, W. Chen, Y. Chen, L. Zhu, W. Yang, L. Wang, W. Hai, Q. Zhao, Z. You, X. Ye, *Nat. Med.* **2021**, *27*, 480.
- [29] H. Chen, Z. Wang, S. Yu, X. Han, Y. Deng, F. Wang, Y. Chen, X. Liu, J. Zhou, J. Zhu, H. Yuan, *J. Hematol. Oncol.* **2021**, *14*, 99.
- [30] a) H. Aghajanian, T. Kimura, J. G. Rurik, A. S. Hancock, M. S. Leibowitz, L. Li, J. Scholler, J. Monslow, A. Lo, W. Han, T. Wang, K. Bedi, M. P. Morley, R. A. Linares Saldana, N. A. Bolar, K. McDauid, C.-A. Assenmacher, C. L. Smith, D. Wirth, C. H. June, K. B. Margulies, R. Jain, E. Puré, S. M. Albelda, J. A. Epstein, *Nature* **2019**, *573*, 430; b) S. Schafer, S. Viswanathan, A. A. Widjaja, W.-W. Lim, A. Moreno-Moral, D. M. DeLaughter, B. Ng, G. Patone, K. Chow, E. Khin, J. Tan, S. P. Chothani, L. Ye, O. J. L. Rackham, N. S. J. Ko, N. E. Sahib, C. J. Pua, N. T. G. Zhen, C. Xie, M. Wang, H. Maatz, S. Lim, K. Saar, S. Blachut, E. Petretto, S. Schmidt, T. Putoczki, N. Guimarães-Camboa, H. Wakimoto, S. van Heesch, et al., *Nature* **2017**, *552*, 110.
- [31] G. P. J. van Hout, L. Bosch, G. H. J. M. Ellenbroek, J. J. de Haan, W. W. van Solinge, M. A. Cooper, F. Arslan, S. C. A. de Jager, A. A. B. Robertson, G. Pasterkamp, I. E. Hoefer, *Eur. Heart J.* **2017**, *38*, 828.
- [32] Ø. Sandanger, E. Gao, T. Ranheim, M. Bliksøen, O. J. Kaasbøll, K. Alfsnes, S. H. Nymo, A. Rashidi, I. K. Ohm, H. Attramadal, P. Aukrust, L. E. Vinge, A. Yndestad, *Biochem. Biophys. Res. Commun.* **2016**, *469*, 1012.
- [33] M. C. Louwe, M. B. Olsen, O. J. Kaasbøll, K. Yang, L. E. Fosshaug, K. Alfsnes, J. D. S. Øgaard, A. Rashidi, V. M. Skulberg, M. Yang, D. de Miranda Fonseca, A. Sharma, J. M. Arosen, E. Schrupf, M. S. Ahmed, C. P. Dahl, T. A. Nyman, T. Ueland, E. Melum, B. E. Halvorsen, M. Bjørås, H. Attramadal, I. Sjaastad, P. Aukrust, A. Yndestad, *JACC: Basic Transl. Sci.* **2020**, *5*, 1210.
- [34] X. Li, Y. Bian, P. Pang, S. Yu, W. Du, *Int. Immunopharmacol.* **2020**, *80*, 106116.
- [35] R. J. Vagnozzi, M. Maillet, M. A. Sargent, H. Khalil, A. K. Z. Johansen, J. A. Schwanekamp, A. J. York, V. Huang, M. Nahrendorf, S. Sadayappan, J. D. Molkentin, *Nature* **2020**, *577*, 405.